Low-frequency fluctuations in the Lang-Kobayashi equations

D. Pieroux and Paul Mandel
Optique Nonlinaire Theorique, Universit Libre de Bruxelles, Campus Plaine Code Postal 231, B-1050 Bruxelles, Belgium
(Received 4 April 2003; published 4 September 2003)

The Lang-Kobayashi equations are simplified by a local analysis that focuses, in the long-delay-time limit, on one pair of mode-antimode only. In the domain of hysteresis between the two steady states, low frequency fluctuations (LFF) can be observed if there is a domain of bistability where both steady states are unstable. The high-frequency oscillations and the drop-offs in the LFF regime are associated with a dynamics close to the unstable upper and lower branch steady states, respectively.

DOI: 10.1103/PhysRevE.68.036204 PACS number(s): 42.65.Sf, 02.30.Ks, 05.45.−a

I. INTRODUCTION

In 1980, Lang and Kobayashi (LK) [1] proposed a simple model to describe the dynamics of a single mode semiconductor laser subject to a coherent optical feedback. The feedback loop is modelled by an external mirror. This creates a passive external cavity. The main feature of the LK model is that the round trip time τ of the laser beam in the external cavity is explicitly taken into account via the delayed complex electric field variable $E(t-\tau)=\rho(t-\tau)e^{i\varphi(t-\tau)}$ fed back in the laser after a round trip in the external cavity. This opens the door to a very complex dynamics since the system phase space has infinite dimension [2]. In particular, it can sustain a chaotic regime displaying low frequency fluctuations (LFF) [3]. They are best observed in the low-pass filtered laser intensity as sudden and irregular drop-offs followed by an intensity recovery [4].

The LFF dynamics associated with the LK model has been the subject of active research for more than two decades (see Ref. [5] for a review and also Ref. [6], which is the latest of an annual series of proceedings on this topic). The purpose of this paper is to analyze the LFF in a simple case where a clear distinction can be made between the causes and the effects of the LFF.

Sano demonstrated numerically that LFF could be described as chaotic itineracy among the many unstable steady states of the system [7]. A similar result was obtained independently by van Tartwijk *et al.* [8]. The question remains, however, to know if that itineracy is the cause or the consequence of the observed LFF.

Using the Sano result, Huyet *et al.* attempted to replace the LK model by a system of ordinary differential equations [9]. To achieve that goal, they considered the small delay time limit, replacing the delayed field amplitude $\rho(t-\tau)$ by its current value $\rho(t)$ and the delayed phase $\varphi(t-\tau)$ by its first-order expansion $\varphi(t)-\tau d\varphi(t)/dt$. The resulting equations have no delayed term any more though the steady states are still those of the full LK model. According to the Sano description, this simplified system was therefore a good candidate to display LFF, which are indeed observed. However, there is no one-to-one correspondence between the solutions of the LK model and those of this reduced model because it is not a consistent asymptotic approximation of the LK equations. The model was further analyzed in Ref. [10] where correlations between the emergence of the LFF and the stability of the steady states were found. Similar correlations are also observed in this paper, but in the opposite limit of a long time delay.

Using a local multiple time scale analysis, Giacomelli and Politi [11,12] showed that the delay differential LK equations are approximated by a partial differential complex Ginzburg-Landau equation in the vicinity of Hopf bifurcations. This approach helps understand the richness of the delay differential equations. Unfortunately it is restricted to the vicinity of the bifurcation point.

In another attempt to simplify the LK model, we have recently proposed to take advantage of the fact that LFF appear for pumping close to threshold, weak feedback level, and large delay [13]. Taking into account that the free carrier lifetime is much larger than the photon lifetime for a typical semiconductor laser, we have adiabatically eliminated the free carrier dynamics, reducing the LK model to a single complex delay equation in the long delay time limit [13]. This amounts to expand the electric field $E_{LK}(t,\tau)$, solution of the LK equations, in inverse fractional powers of the delay time τ as $E_{LK}(t,\tau)=\tau^{-1/2}E(t)+O(\tau^{-1})$. Numerical simulations showed that the reduced LK model for $E(t)$ is still able to sustain LFF. Its advantage over the complete LK model comes from the elimination of the laser relaxation mechanism from the system dynamics: the reduced model no longer presents the numerical stiffness of the LK model, allowing a much simpler and faster numerical integration. As noted in Ref. [13], the long delay time limit is regular, which implies that all solutions of the reduced model are also solutions of the full model in the limit of a weak feedback and for pumping close to the solitary threshold, the converse being equally true. Simplifying further the reduced LK model is thus a sensible strategy to determine properties of the LFF. In this paper, we show that the reduced model can be further simplified to retain only one branch of finite intensity steady states. In the language of the LK equations, this amounts to select one particular external cavity mode and neglect all the others. The resulting system still displays LFF and is simple enough to allow for a characterization of this LFF attractor, which is the purpose of this paper.

The plan of the paper is as follows. In Sec. II, we derive a simplified model from the reduced LK model. In Sec. III, analytical results are presented, followed by numerical results in Sec. IV. A detailed discussion of LFF is presented in Sec. V before we conclude in Sec. VI with a clear distinction between the causes and the effects of LFF in the frame of the

simplified single mode deterministic model analyzed in this paper.

II. MODEL DERIVATION

The dynamics of the complex electric field $E(t)=\rho(t)e^{i\varphi(t)}$ of a semiconductor laser pumped exactly at the solitary laser threshold and subject to a weak coherent optical feedback with a large delay can be described by the reduced LK model [13]:

$$\frac{dE}{dt}=-(1+i\alpha)|E|^2E+\eta E(t-1), \tag{1}$$

in complex form, or

$$\frac{d\rho}{dt}=-\rho^3+\eta\hat{\rho}\cos(\varphi-\hat{\varphi}), \tag{2}$$

$$\rho\frac{d\varphi}{dt}=-\alpha\rho^3-\eta\hat{\rho}\sin(\varphi-\hat{\varphi}), \tag{3}$$

in real form, where the dimensionless time t is expressed in units of the delay time, α is the linewidth enhancement factor, and $\eta\geqslant 0$ is the feedback strength. The delay appears through $\hat{\rho}\equiv\rho(t-1)$ and $\hat{\varphi}\equiv\varphi(t-1)$. Most electronic devices are too slow to record the instantaneous laser intensity $|E|^2=\rho^2$. Therefore, to compare theoretical results with experimental results, it is necessary to introduce a low-pass filtered intensity I given by

$$\frac{dI}{dt}=(\rho^2-I)/\tau_f, \tag{4}$$

where τ_f is the time constant of the filter. This amounts to a time averaging of ρ^2, which is precisely what a slow detector does.

The reduced LK equations (2) and (3) have steady, periodic, quasiperiodic, and chaotic solutions, among which the LFF type of solutions. For a moderate η, multiple dynamical regimes coexist, with multistability between some of them. An example of LFF regime is illustrated in Fig. 1. In this regime, Fig. 1(b) shows that the phase difference $\varphi-\hat{\varphi}$ remains mostly located in the vicinity of $\varphi-\hat{\varphi}=-13\approx -4\pi$, which corresponds to one specific unstable steady state. This suggests a two-step reduction of the LK equations to focus on that particular branch of steady states and the dynamics connected to that branch. First, we introduce a new phase variable $\varphi=\phi-4\pi t$. As a result, $\phi-\hat{\phi}$ remains most of the time close to zero. Second, we replace the trigonometric functions by their truncated Taylor's expansion. The resulting simplified model is thus given by

$$\frac{d\rho}{dt}=-\rho^3+\eta\left[1-\frac{1}{2}(\phi-\hat{\phi})^2\right]\hat{\rho}, \tag{5}$$

$$\rho\frac{d\phi}{dt}=4\pi\rho-\alpha\rho^3-\eta(\phi-\hat{\phi})\hat{\rho}. \tag{6}$$

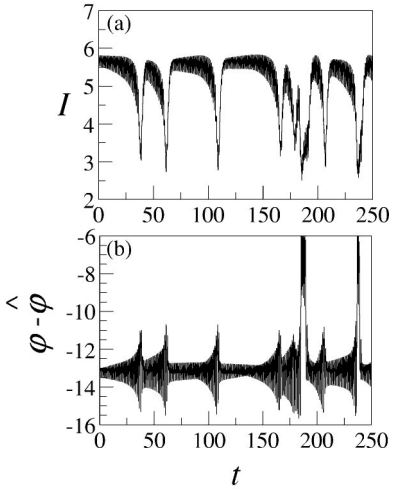

FIG. 1. Low frequency fluctuations obtained by numerical integration of the reduced LK model, Eq. (1). Parameters are $\eta=6.95$ and $\alpha=3$. The intensity is filtered according to Eq. (4) with $\tau_f=1$.

Because of the series truncation, the simplified model (5) and (6) are obviously not equivalent to the reduced LK model. Nevertheless, using the same parameters as in Fig. 1, Fig. 2 shows that it can still sustain LFF. Comparing the two sets of time traces reveals qualitative differences. In particular, the two pulses where $\phi-\hat{\phi}$ reached -6, seen in Fig. 1, are absent in the simplified model. This is normal since these excursions correspond to values of $\phi-\hat{\phi}$ for which the truncated series is not a good approximation of the trigonometric functions anymore. This is why the LFF produced by the reduced LK model (1) are more irregular than those of the simplified model (5) and (6).

III. ANALYTICAL RESULTS

As explained in the Introduction, the main motivation for simplifying the reduced LK model is to simplify its bifurca-

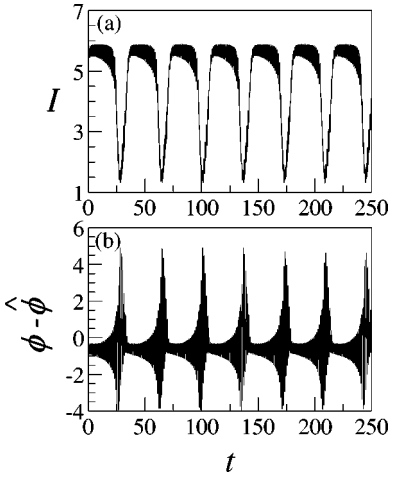

FIG. 2. Low frequency fluctuations obtained by numerical integration of the simplified model, Eqs. (5) and (6). The intensity is filtered according to Eq. (4) with $\tau_f=1$. Same parameters as in Fig. 1.

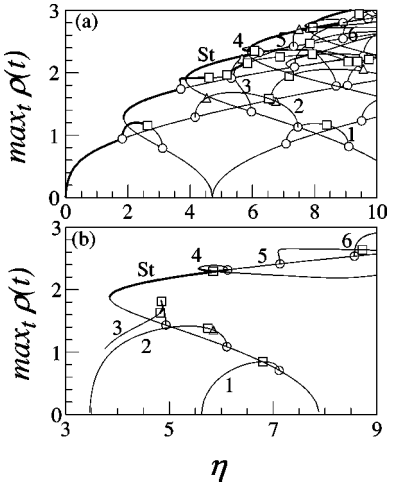

FIG. 3. Bifurcation diagrams for $\alpha=3$. The steady branches emerge from the zero solution, the periodic branches emerge from the steady branches. Thick (thin) lines correspond to stable (unstable) regime. Labels St and 1–6 designate the same branches in both diagrams. Circles (squares) are primary (secondary) Hopf bifurcations leading to periodic (quasiperiodic) solutions. Triangles are period doubling bifurcations. (a) Reduced LK model, Eq. (1). (b) Simplified model, Eqs. (5) and (6).

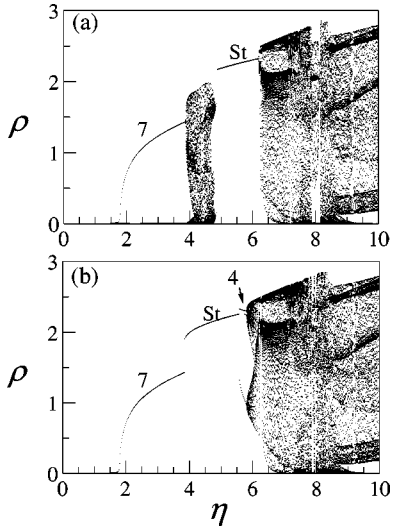

FIG. 4. Bifurcation diagram for $\alpha=3$ obtained by numerical integration of the simplified LK model, Eqs. (5) and (6). The extremum values of $\rho(t)$ are plotted, i.e., values for which $d\rho/dt$ vanishes: (a) Forward, (b) backward sweeping of η. Labels: St, 3, and 4 correspond to the stable section of the same branches in Fig. 3(b); 7 indicates another periodic branch absent from Fig. 3(b).

tion diagram without disabling LFF generation. The bifurcation diagrams of the reduced model (2) and (3) and of the simplified model (5) and (6) are displayed in Figs. 3(a) and 3(b), respectively. A detailed description of the bifurcation diagram shown in Fig. 3(a) for the reduced LK model is found in Ref. [13]. For the simplified model, the branch labeled St in Fig. 3(b) corresponds to steady solutions of the form $\rho(t)=\rho_s$ and $\varphi(t)=\omega_s t$. In the LK terminology, the upper (lower) part of the branch corresponds to modes (antimodes) of the external cavity. The steady solutions are

$$\omega_s=\frac{\eta+1}{\alpha\eta}\pm\frac{\sqrt{1+\eta[2\alpha(\alpha\eta-4\pi)+2+\eta]}}{\alpha\eta}, \tag{7}$$

$$\rho_s^2=(2-\omega_s^2)\,\eta/2. \tag{8}$$

The highest values of ω_s belong to the lower branch steady state. There are only three possibilities: (i) no steady state solution [leftmost part of Fig. 3(b)]; (ii) only one steady state [rightmost part of Fig. 3(b)]; (iii) two coexisting steady states [central part of Fig. 3(b)]. This contrasts with the reduced LK model for which an increasing number of modes and antimodes coexist for increasing η. For instance, with the value $\eta=6.95$ that was used in Figs. 1 and 2, the reduced LK model has seven coexisting steady solutions (of which only one is stable), while the simplified model has only two coexisting steady solutions, both unstable. Equations (7) and (8) also reveal that for $\alpha<2\pi/(2\sqrt{2}\pi-1)\approx 0.797$, the steady branch emerges supercritically and has no turning point. However, for conventional semiconductor lasers, experimental values of α are in the range 3–5. For quantum well lasers, $\alpha\simeq 2$, and for quantum dot lasers $\alpha\simeq 1$. Therefore, we do not consider the supercritical case in this paper. The branch of finite intensity solutions starts at $\eta=2\sqrt{2}\pi-1$ with $\rho_s=0$ and $\omega_s=\sqrt{2}$. Following that branch, η and ω_s decrease while ρ_s increases. There is a turning point for $\omega_s=4\pi-\sqrt{(16\pi^2\alpha-2\alpha-8\pi)/\alpha}$. Beyond the turning point, ω_s continues to decrease while η and ρ_s increase. Asymptotically, for $\eta\to\infty$, it is easy to verify that $\omega\to(1-\sqrt{1+2\alpha^2})/\alpha<0$ and $\rho_s\approx(1-\omega_\infty^2)\,\eta/2\to\infty$.

IV. NUMERICAL RESULTS

To complement the analytical results, we have used the numerical package DDEBIFTOOL [14] to locate the Hopf bifurcations on the branches of steady states. We found three of them on the lower part of the steady branch and three others on the upper steady branch for $\eta\leqslant 9$. There are many more Hopf bifurcations for larger values of η. As seen in Fig. 3(b), the stable section of the upper steady branch ends at a Hopf bifurcation. Branches of periodic solutions emerge from the Hopf bifurcations. Secondary Hopf bifurcations were found on each of the six periodic branches of Fig. 3(b). All periodic branches are unstable, with the exception of two small segments on the branches labeled 3 and 4. These segments are limited by a turning point and a secondary Hopf bifurcation. Numerical integration of the simplified equations (5) and (6) shows that stable quasiperiodic regimes emerge from these two secondary Hopf bifurcations. Unstable quasiperiodic regimes emerge from the other secondary Hopf bifurcation.

The numerical package DDEBIFTOOL is able to follow only steady and periodic branches, irrespective of their stability. We have used direct numerical time integration, sweeping η, to obtain the quasiperiodic and chaotic branches. To detect multistable regimes, two sweepings are performed: one with increasing η [Fig. 4(a)] and one with decreasing η [Fig. 4(b)]. To avoid problems related to the slow passage through bifurcations [15,16], a small perturbation was added to ρ

each time η was updated, and the system was let to relax before measuring the local extrema of ρ. With this procedure, we found one more periodic branch. It is labeled 7 in Fig. 4 to avoid confusion with the periodic branches of Fig. 3. It starts at $\eta \approx 1.8$ and remains stable up to $\eta \approx 3.9$ where the regime becomes quasiperiodic. For higher η, there is a transition towards a chaotic regime, followed by a quasiperiodic regime. At $\eta \approx 4.84$, there is an inverse Hopf bifurcation to a periodic regime. The periodic branch becomes unstable at $\eta \approx 4.86$ and the system jumps to the steady state branch. This small periodic branch corresponds to the small stable section of the periodic branch 3 of Fig. 3. The stable part of branch 4 of Fig. 3 is also observed in Fig. 4(b), while it is absent from Fig. 4(a) because of the multistability existing with the steady state. Finally, it is seen that for η higher than 6, the system is chaotic.

Let us compare the bifurcation diagram of the reduced LK model, Fig. 3(a), and that of the simplified model, Fig. 3(b). Although multiple steady branches are seen in Fig. 3(a), only one steady state branch exists in Fig. 3(b), a direct consequence of the manipulations leading to the simplified equations. The upper part of the steady branch, labeled St in Fig. 3(a), matches well the corresponding branch of the simplified model. We checked that defining $\phi = \varphi + 2(n-1)\pi t$ with $n = 1, 2, \ldots$ selects the nth upper branch. The lower part of the steady state branch, characterized by the largest ω_s, suffers the largest deformation. For instance, the connection to the zero solution occurs at $\eta = 7\pi/2 = 10.996$ for the reduced LK model, while it occurs at $\eta = 2\sqrt{2}\pi - 1 \approx 7.886$ for the simplified model.

There is very good agreement between the two models for the number and the position of the Hopf bifurcations. For the range of η plotted in Fig. 3(b), six Hopf bifurcations are found, three on the upper part of the branches and three on the lower ones. The shape and stability of the periodic solutions close to the Hopf bifurcations that emerge on the upper steady state branch are similar for the reduced and the simplified models. However, branches 1–3 display marked differences. In the case of the reduced LK model, branches 1 and 2 form bridges between the selected steady branch and two other branches. Because the latter branches have been eliminated in the simplified model, the corresponding periodic branches have a different topology away from the bifurcation points and eventually collide with the zero solution. Concerning the two branches 3, they both emerge subcritically but then evolve very differently in both figures. Due to a unresolved numerical problem, we failed at continuing further the unstable branches 3 for both figures.

V. LFFs ATTRACTOR

In this section, we describe the LFFs in the simplified model. The first problem to solve is how to analyze complex attractors of the simplified model. There are three informations that can be obtained easily from numerical simulations: the phase ϕ, the instantaneous intensity ρ^2, and the filtered intensity I. These three informations are used, for instance, in Fig. 5 for two segments of the same time series generated by Eqs. (5) and (6). From top to bottom, these figures display

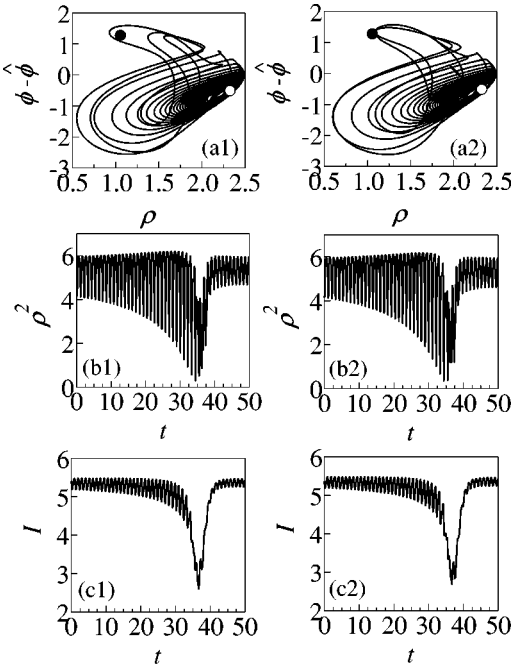

FIG. 5. Phase space portrait, instantaneous intensity (ρ^2), and filtered intensity (I) for two different time intervals of the same solution of the simplified model. Parameters are $\alpha = 3$, $\eta = 6.2$, and $\tau_f = 1$.

the portrait of the attractor in the phase plane ($\phi - \hat{\phi}, \rho$), the instantaneous intensity versus time, and the filtered intensity versus time. The two steady states are indicated in the phase portraits: the white dot for the upper branch and the black dot for the lower branch. It is seen that the high-frequency oscillations, which have the same frequency for ρ^2 and for I, correspond to the motion in the vicinity of the upper branch steady state, while the drop-offs correspond to segments of the trajectory in the vicinity of the lower branch steady state. Comparing Figs. 5(a1) with 5(c1) and 5(a2) with 5(c2) shows that there is a one-to-one correspondence between the trajectories in the vicinity of the black dot (lower branch steady state) and the fine structure of the drop-off. Thus, comparing the phase portrait and the averaged intensity is a sensible way to analyze the attractor and does not introduce a bias.

Important steps are illustrated in Figs. 6 and 7. In Figs. 6(a)–6(c) and 7(a)–7(c), the upper branch steady state (white dot) is stable and coexists with the stable periodic and quasiperiodic solutions. The two Hopf bifurcations on the upper branch, leading to branches labeled 4 and 5, occur at $\eta \simeq 6.145$ and $\eta \simeq 7.129$. On the lower branch, the three Hopf bifurcations, leading to branches 1, 2, and 3, occur at $\eta \simeq 7.115$, 6.11, and 4.931, respectively. The lower branch vanishes at $\eta = 2\sqrt{2}\pi - 1 \simeq 7.886$.

Figures 6(a) and 7(a) display two complementary views of the periodic solution located on the stable section of branch 4 in Fig. 3(b). Increasing η, this solution is destabilized by a secondary Hopf bifurcation from which a branch of quasiperiodic solutions emerge supercritically [Figs. 6(b) and 7(b)]. Increasing η, the amplitude of the quasiperiodic solution increases while the quasiperiodic intensity temporal

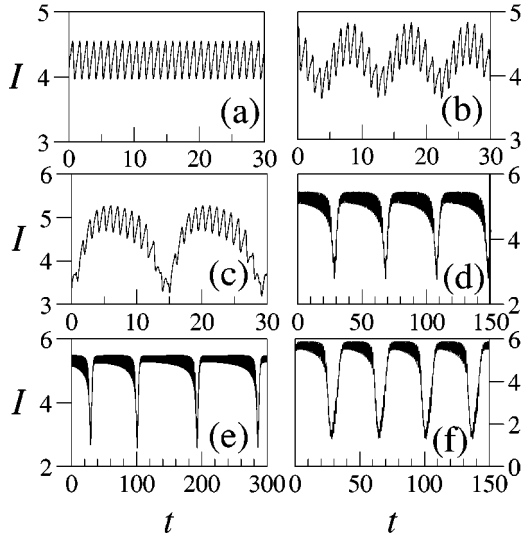

FIG. 6. Intensity time traces for $\alpha=3$ and $\tau_f=1$ illustrating the appearance and development of the LFF attractor and obtained by numerical integration of the simplified model, Eqs. (5) and (6). Values of η: (a) 5.75, (b) 5.85, (c) 6.04, (d) 6.15, (e) 6.25, and (f) 6.95.

pattern is continuously deformed. A nascent drop-off results from the steepening of the minimum in the quasiperiodic solution. At $\eta=6.04$, there is a qualitative change: the torus of quasiperiodic solutions is no longer uniformly covered [Figs. 7(c)]. The transition between the two regimes is continuous. These three figures represent the periodic and quasiperiodic attractors that coexist with a stable steady state on the upper branch.

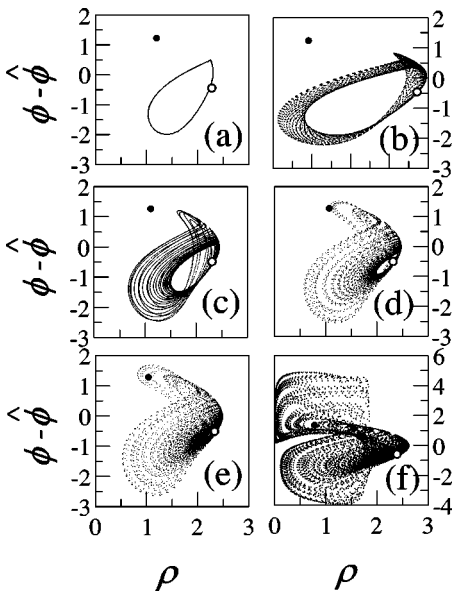

FIG. 7. Phase diagrams illustrating the apparition and development of the LFF attractor and obtained by numerical integration of the simplified model, Eqs. (5) and (6). Same parameters as in Fig. 6. The white (black) dot is at the position of the upper (lower) steady state. The lower steady state is unstable. The upper steady state is stable only for parts (a)–(c).

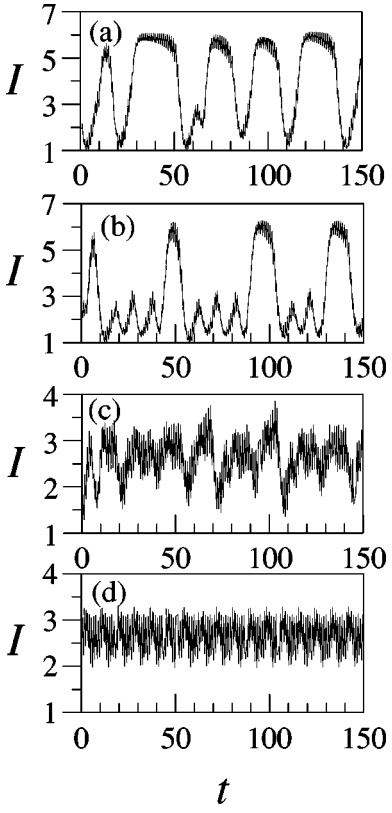

FIG. 8. Intensity time traces illustrating the progressive disappearance of the LFF regime obtained by numerical integration of the simplified model, Eqs. (5) and (6). Values of η: (a) 7.5, (b) 8, (c) 8.5, (d) 9. Other parameters are as in Fig. 1.

As the upper branch steady state becomes unstable, there is a qualitative change in the solutions and the LFF appear. In the domain of η covered by Figs. 6(d), 6(e), 7(d), and 7(e), the manifold associated with the upper branch has two unstable directions and an infinity of stable directions, while the manifold associated with the lower branch has five unstable directions and an infinity of stable directions. The filtered intensity displays the typical LFF structure. Increasing further η leads to the accentuation of the drop-off amplitude and an increase of the average time between the drop-offs [Fig. 6(d)]. The relation between η and the average delay between two drop-offs is not monotonic: for $\eta=6.25$, [Fig. 6(e)], the average duration between the drop-offs reaches its maximum, slightly less than 100 delay times. Figure 6(e) also shows that the plateau duration as well as the depth of the drop-offs vary significantly in a single run. A further increase of η leads to a decrease of the plateau duration and to an increase of the drop-off amplitude [Fig. 6(f)].

Increasing the feedback strength leads to the progressive destruction of the LFF and its replacement by another chaotic attractor, as shown in Fig. 8. Figure 8(a), for $\eta=7.5$, shows that the LFF attractor becomes more irregular, with a new small scale structure appearing. For $\eta=8$ [Fig. 8(b)], the system jumps chaotically between two coexisting attractors. Finally, no more intensity recovery occurs [Fig. 8(c) for $\eta=8.5$], and the LFF dynamics is totally gone. This regime has been called coherence collapse in the case of the LK

model [17]. Increasing further the feedback leads to a decrease of the intensity variation [Fig. 8(d) for $\eta=9$]. We have not analyzed this chaotic attractor since the simplified model is not to be taken seriously in that domain of parameters. However, the mechanism through which the LFF attractor disappears and the coarse grained structure of the emerging chaotic attractor are in qualitative agreement with what can be observed for the complete LK equations.

VI. CONCLUSION

Starting from the reduced version of the LK model valid in the long delay time limit, we derived a simplified model based on the numerical observation that the phase difference $\varphi-\hat{\varphi}$ remains most of the time close to a multiple of 2π, even in the LFF regime. The result of the simplification is fully appreciated by comparing the bifurcation diagrams before and after simplification: from the infinitely many steady branches, the simplification scheme amounts to selecting only one connected pair of them. Only the periodic, quasiperiodic and chaotic attractors connected to the two selected branches remain. Few analytical results can be derived. Using the numerical continuation package DDEBIFTOOL, the branches of periodic solutions emerging from the steady branch have been described. Quasiperiodic and chaotic solutions have been found by numerical simulations.

From the analysis in Sec. V, it is seen that necessary conditions for the occurrence of LFF for this class of delay differential equations are (1) the occurrence of steady state bistability and (2) instability of both steady states. The domain of LFF does not strictly coincide with the bistability domain: LFF begin for η slightly larger than the lower bound of the hysteresis (where the quasiperiodic solutions are observed) and extend slightly beyond that domain. The only parameters that are necessary to account for the LFF are the feedback strength η and the phase-amplitude coupling α. Two direct consequences of this analysis are that (i) the relaxation oscillations which are present in the LK equations are by no means related to the LFF phenomenon: LFF can occur with or without relaxation oscillations since they are absent in the reduced and in the simplified models. This property was already explained previously [13]. (ii) The chaotic itineracy described by Sano is a consequence of LFF in the presence of multiple coexisting steady branches and not a cause of the LFF.

The results obtained in this paper do not rule out the influence of other parameters. The only statement which is made here is that LFF can be explained in terms of a single mode deterministic theory that contains only one pair of mode-antimode, which have a domain of bistability and are both unstable. The smooth recovery observed after a drop-off is consistent with the experimental results. It was shown that, after averaging the output signal over many samples, the recovery is stepwise [18]. However, the height of the steps decreases with increasing delay time and therefore it is natural that the recovery appears as continuous in an asymptotic theory based on an expansion in inverse powers of the delay time. Likewise, noise is not a prerequisite for the occurrence of LFF, as assumed in some previous studies [19–21]. Of course, experimental results are necessarily affected by noise, and therefore experimentally observed LFF will display a number of features that pertain to noisy systems. But again, we stress that these are consequences and not causes of the LFF. The same is true for the relaxation oscillations. Finally, it should be noticed that the correlation between the LFF attractor and the instability of the upper branch steady state is similar to the mechanism found in the more complex situation analyzed in the short delay time limit [10].

ACKNOWLEDGMENTS

Fruitful discussions with E. Viktorov are gratefully acknowledged. This research was supported in part by the Fonds National de la Recherche Scientifique and the Interuniversity Attraction Pole program of the Belgian government.

[1] R. Lang and K. Kobayashi, IEEE J. Quantum Electron. **QE-16**, 347 (1980).
[2] J.D. Farmer, Physica D **D4**, 366 (1982).
[3] T. Morikawa, Y. Mitsuhashi, and J. Shimada, Electron. Lett. **12**, 435 (1976).
[4] C. Risch and C. Voumard, J. Appl. Phys. **48**, 2083 (1977).
[5] G.H.M. van Tartwijk and D. Lenstra, Quantum Semiclassic. Opt. **7**, 87 (1995).
[6] *Physics and Simulation of Optoelctronic Devices IX*, edited by Y. Arakawa, P. Blood, and M. Osinski, SPIE Proceedings, Vol. 4283 (SPIE, Bellingham, 2001).
[7] T. Sano, Phys. Rev. A **50**, 2719 (1994).
[8] G.H.M. van Tartwijk, A.M. Levine, and D. Lenstra, IEEE J. Sel. Top. Quantum Electron. **1**, 466 (1995).
[9] G. Huyet *et al.*, Opt. Commun. **180**, 339 (2000).
[10] A. Prasad, Y.-C. Lai, A. Gavrielides, and V. Kovanis, J. Opt. B: Quantum Semiclassical Opt. **3**, 242 (2001).
[11] G. Giacomelli and A. Politi, Phys. Rev. Lett. **76**, 2686 (1999).
[12] G. Giacomelli and A. Politi, Physica D **117**, 26 (1998).
[13] D. Pieroux and P. Mandel, Phys. Rev. E **67**, 056213 (2003).
[14] K. Engelborghs, Report No. TW-305 (unpublished).
[15] P. Mandel, *Theoretical Problems in Cavity Nonlinear Optics* (Cambridge University Press, Cambridge, 1997).
[16] S.M. Baer, T. Erneux, and J. Rinzel, SIAM (Soc. Ind. Appl. Math.) J. Appl. Math. **49**, 55 (1989).
[17] D. Lenstra, B.H. Verbeck, and A.J. den Boef, IEEE J. Quantum Electron. **QE-21**, 674 (1985).
[18] Y. Liu, P. Davis, and Y. Takiguchi, Phys. Rev. E **60**, 6595 (1999).
[19] M. Giudici *et al.*, Phys. Rev. E **55**, 6414 (1997).
[20] M.C. Eguia, G.B. Mindlin, and M. Giudici, Phys. Rev. E **58**, 2636 (1998).
[21] A. Hohl, H.J.C. van der Linden, and R. Roy, Opt. Lett. **20**, 2396 (1995).